Chemical Science

ROYAL SOCIETY OF CHEMISTRY

EDGE ARTICLE

View Article Online
View Journal

Check for updates

Cite this: DOI: 10.1039/d6sc03833f

All publication charges for this article have been paid for by the Royal Society of Chemistry

Lipid nanoparticle formulations including stereochemically defined glycomacromolecules for delivery of saRNA

Jonas Becker, †[a] Beatriz Dias-Barbieri, †[b] Robin J. Shattock*[b] and C. Remzi Becer *[a]

Targeted and efficient delivery of nucleic acid therapeutics (NATs) is one of the major challenges in the development of next generation vaccine formulations. Glycosylated lipid nanoparticles (LNPs) utilising mannose as an active targeting ligand have the potential to improve NAT based treatments owing to their ability to bind to carbohydrate-binding protein receptors associated with immune cells. Addressing these receptors specifically results in improved cellular uptake and therefore more efficient delivery of the RNA cargo. Glycomacromolecules (GMs) with defined valency and configuration can distinguish between receptors and enhance the functionality of LNP-based formulations by pinpointing different cell types and enabling specific uptake. Therefore, in this study a library of nine discrete mannosylated GMs with a distinct stereoconfiguration were synthesised and incorporated into LNP membranes *via* cholesterol anchors. Established LNP formulations based on C12-200 are equipped with these GMs on their surface and evaluated for their biological performance. Surface plasmon resonance spectrometry (SPR) has been employed to investigate their binding properties with a variety of human lectins, to elucidate the avidity of both the individual GMs and the LNPs to the receptors, revealing specific lectin interactions. Additionally, the successful delivery of self-amplifying RNA (saRNA) in the glycosylated LNPs is analysed for cellular transfection efficiency in cell lines such as HEK293T/17, THP-1 and BMDC, and transfection efficiency is also evaluated in an *ex vivo* human skin explant model.

Received 7th May 2026
Accepted 20th May 2026

DOI: 10.1039/d6sc03833f

rsc.li/chemical-science

Open Access Article. Published on 15 June 2026. Downloaded on 6/15/2026 11:32:43 PM. This article is licensed under a Creative Commons Attribution-NonCommercial 3.0 Unported Licence.

Introduction

Lipid nanoparticles (LNPs) have emerged as a promising strategy to deliver nucleic acids in pharmaceutics, leading to FDA-approved treatments such as Patisiran and the Covid-19 mRNA vaccines.[1,2] These breakthroughs are the result of a vast investigation of LNP formulations for gene delivery in vaccines, protein replacement and gene silencing.[3,4] LNPs have proven to be effective, easy to scale up and safer than viral vectors.[5–7] They have especially achieved the successful delivery of otherwise unstable mRNA, rendering a wide variety of potential therapeutic applications.[8] Similarly, the utilisation of self-amplifying RNA (saRNA) has raised attention, as it encodes a replicase that can make copies of the original RNA strand, requiring significantly lower doses for an immune response than mRNA.[9–12] One crucial limitation of LNPs, however, is presented by their fate to ultimately end up in the liver, when injected intravenously, limiting their therapeutic versatility.[13] Local administration, *e.g.* intramuscular, can circumvent this issue, but for future developments, tissue-specific targeting is desired to precisely tailor immune responses to the area of interest.[5,14,15] Evidently, the chemical composition of the chosen formulation, in particular the helper lipids, PEGylation, size and protein corona formation can induce an effect for passive organ targeting.[16–20] Moreover, active targeting approaches with saRNA have been realised by Goswami *et al.*, showing the enhanced uptake of mannosylated LNP systems by antigen-presenting cells (APCs).[21,22] Notably, the onset of immune response in both *in vitro* and *in vivo* was observed to be more rapid with mannose on the surface of LNPs. This carbohydrate-mediated targeting relies on the multivalent interaction with carbohydrate-binding receptors (lectins), increasing the efficiency of cellular uptake. Furthermore, glycosylated delivery systems for nucleic acids can recognise specific cell types according to the lectins expressed on their cell surface.[23–25]

Herein, we investigated the effect of glycosylation and variation of ligand stereochemistry on cellular transfection. This approach does not only make use of mannose-mediated targeting but also takes the conformation of the targeting molecules into account. Precise glycomacromolecules (GMs) with a defined tacticity and multivalency have been utilised, as they exhibit selective binding to mannose-binding lectins.[26] The

[a]*Department of Chemistry, University of Warwick, Coventry CV4 7AL, UK. E-mail: Remzi.Becer@warwick.ac.uk*

[b]*Department of Infectious Diseases, Imperial College London, London W21PG, UK. E-mail: r.shattock@imperial.ac.uk*

† These authors contributed equally to this work.

© 2026 The Author(s). Published by the Royal Society of Chemistry

Open Access Article. Published on 15 June 2026. Downloaded on 6/15/2026 11:32:43 PM. This article is licensed under a Creative Commons Attribution-NonCommercial 3.0 Unported Licence.

influence of stereoconfiguration on biological performance of LNP formulations presents an unprecedented attempt to improve the cellular targeting selectivity, which remains an issue in carbohydrate-mediated uptake.[27–29]

For this task, a library of nine GMs comprising two, four or eight mannose units featuring a distinct stereoconfiguration (*R* or *S*) was synthesised. Cholesterol moieties are introduced into the structures, acting as anchoring units for the incorporation into the lipid layer of LNPs (Fig. 1). The resulting formulations were tested in cellular transfection and cytotoxicity assays with human embryonic kidney (HEK) 293T/17, Tohoku Hospital Pediatrics-1 (THP-1) and bone-marrow-derived dendritic cells (BMDCs), with transfection efficiency also evaluated in human skin explants *ex vivo*. Glycosylated LNPs exhibited no cytotoxicity, comparable levels of saRNA expression to control samples in human cell lines and a tendency of increased expression in human skin explants. Taken together, these results demonstrate the promising applicability of such systems for selective delivery of saRNA LNP to immune cells, especially in an ex vivo model of skin explants with previously demonstrated translational potential, which should be further explored.

Results and discussion

Synthesis and characterisation of cholesterol-containing glycomacromolecules

A well-established synthesis approach to produce unimolecular macromolecules with a defined stereochemistry has been developed by Johnson and co-workers.[30–32] Therein, iterative exponential growth (IEG) is employed to elongate the overall chain length of the oligomers by copper-catalysed azide–alkyne cycloaddition (CuAAC). Whilst one chain end presents a bromide, which can be readily converted into an azide moiety, the other end contains a protected alkyne, allowing stepwise CuAAC coupling of the precursors. This leads to a new triazole formation with each cycle. The scaffold grows by 2^n, where n represents the number of IEG cycles performed. Notably, this route renders macromolecules with total control over the chain length and stereoconfiguration, utilising chiral precursors. An adaptation of this strategy was used in this study to fabricate allyl-containing oligomers, in which the alkyne chain end is functionalised with 3-(13-azido-5,8,11-trioxa-2-azatridecanoate) cholesterol (cholesteryl-TEG-azide) (Fig. 2A). The valency of allyl bonds, *i.e.* the number of carbohydrate units in the final compounds, was aimed at two, four and eight to examine the effect of ligand multivalency on the performance of the desired formulations. Additionally, all compounds were synthesised in three stereoconfigurations: racemic, *R* and *S*. The nomenclature of the enantiopure versions of this library (*R* and *S* configurations) was adapted from the literature, namely that the letter represents the configuration of the corresponding epichlorohydrin precursors used.[31]

The oligotriazoles produced after the IEG cycles (IEGmers) were deprotected in the presence of tetrabutylammonium fluoride (TBAF), upon which the CuAAC catalytic system consisting of CuBr/PMDETA was added in a one pot reaction with cholesteryl-TEG-azide.[33,34] ^{1}H NMR (Fig. 2B) reveals the characteristic cholesterol peak pattern between 0.6 and 2.8 ppm and a new aromatic proton at 7.76 ppm, which can be assigned to the additional triazole ring formed. In order to introduce lectin recognition properties, 2,3,4,6-tetra-*O*-acetyl-1-thio-β-D-mannopyranose (Ac_4ManSH) was chosen as a mannose reagent to functionalise the double bonds *via* thiol–ene chemistry.[35] Quantitative consumption of double bonds was monitored by ^{1}H NMR (Fig. 2B) and was achieved at a molar ratio of allyl/AIBN/Ac_4ManSH = 1/0.25/6 at 70 °C overnight. Ultimately, complete deacetylation of the mannose units was observed in the spectra of the final products.

To examine the integrity of the chiral information of the GMs after they had undergone several synthesis steps, circular dichroism (CD) spectroscopy was employed (Fig. 2C). The spectra were collected in water at neutral pH and showed significant differences depending on the chirality of the chosen precursors. Whilst **4*R*** and **8*R*** exhibited a distinctive negative band between 194 and 247 nm, **4*S*** and **8*S*** gave a negative signal

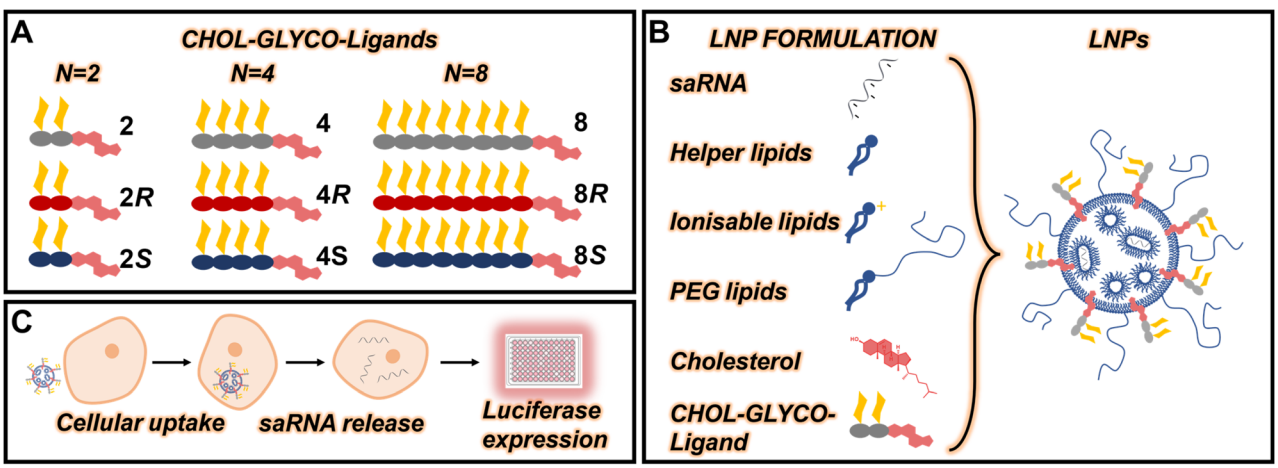

Fig. 1 Illustration of the scope of this study. (A) Library of glycomacromolecules with defined configuration and valency. (B) Components of the LNP formulations used in this study. (C) Illustration of cell transfection experiments performed.

© 2026 The Author(s). Published by the Royal Society of Chemistry

Open Access Article. Published on 15 June 2026. Downloaded on 6/15/2026 11:32:43 PM.
This article is licensed under a Creative Commons Attribution-NonCommercial 3.0 Unported Licence.

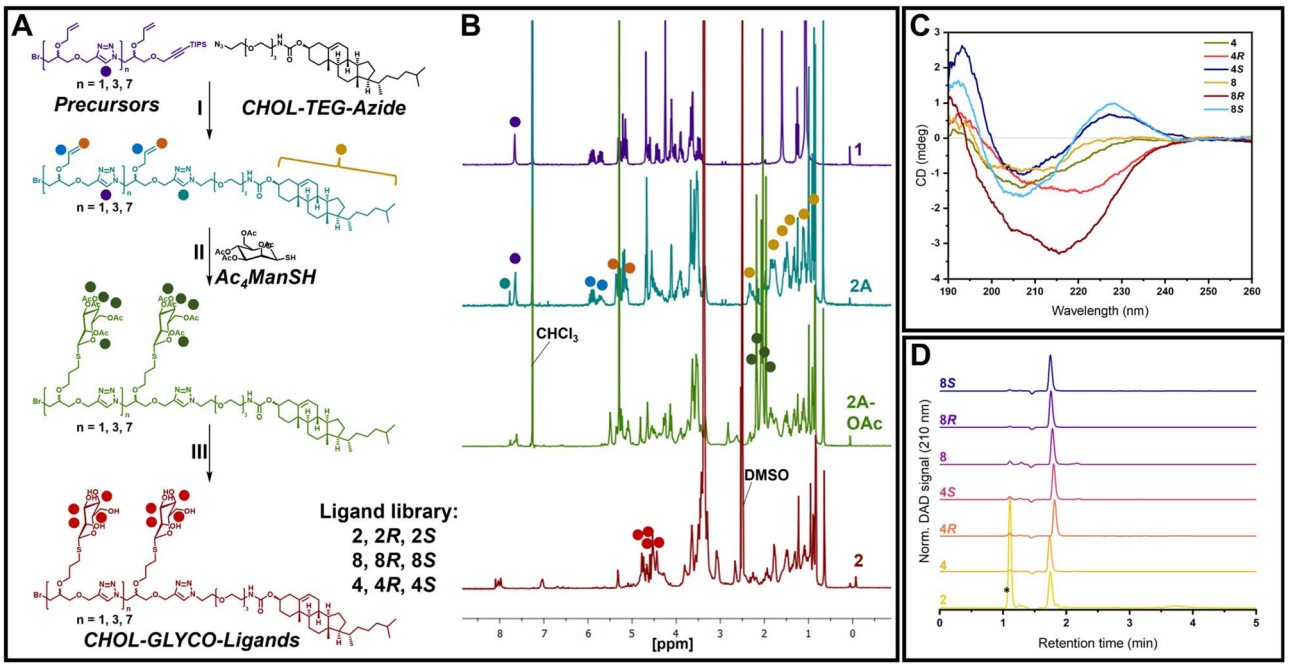

Fig. 2 Synthesis and characterisation of the functionalisation of IEGmers with cholesteryl-TEG-azide and subsequent glycosylation. (A) Synthetic scheme (I) (1) TBAF, THF, 2 h, r.t. (2) CuBr/PMDETA, THF, 45 °C, 18 h. (II) AIBN, MeCN, 70 °C, 18 h. (III) NaOMe, MeOH, r.t., 2 h. (B) Stacked representative ^{1}H NMR spectra (400 MHz, $CDCl_3$ or DMSO-d6) of each synthesis step. (C) Overlaid CD spectra of GMs in H_2O. (D) Normalised HPLC traces (DAD, 210 nm, eluent: H_2O/MeCN 1% (+0.04% TFA)) of the final GMs. *System peak observed in higher intensity due to low sample concentration.

in the range from 197 to 219 nm but also showed a positive band between 220 to 245 nm. Racemic samples **4** and **8** both resulted in a CD response that lies in between the two corresponding enantiopure counterparts. From this investigation it can be deduced that the stereoconfiguration of the cholesterol-containing GMs modulates their three-dimensional conformation and likely influences the selective interactions of the GMs with biomolecules, such as lectin receptors.

HPLC investigation of the final cholesterol-containing GMs (Fig. 2D) shows a single peak eluting within 2 minutes of the chosen isocratic elution method. The non-polar component of the eluent mixture (acetonitrile) was kept at a low amount of 1%, to maximise the interaction of the sample with the column, however, the polar nature of the carbohydrate-carrying compounds prevents a strong interaction with the hydrophobic C18 column, resulting in low retention times.[36,37] Furthermore, all compounds elute at a very similar time, regardless of molecule size or carbohydrate to cholesterol ratio. Nevertheless, the synthesised GMs all showed an excellent purity as observed on the HPLC chromatograms and seemed therefore suitable for further biological experiments.

High resolution electron-spray microscopy (HR ESI-MS) of the final compounds was conducted to confirm their molecular structure and the integrity of the cholesterol double bond between carbons 5 and 6 of the steroid. Thiol–ene addition to this bond is not intended, as it could lead to a change in polarity of the cholesterol moiety and thus alter the characteristics required for incorporation into lipid membranes. Comparison of the spectra of GMs **2** and **4** with the predicted molecular weights (SI, Fig. S13 and S14) suggests that the cholesterol double bond remains intact throughout the reaction procedure, as the peak patterns of the sample measurement are in good agreement with the predicted patterns of molecular ion peaks $[M + Na]^+$ and $[M + 2Na]^{2+}$ for **2** as well as $[M + 2H]^{2+}$ and $[M + 2H + Na]^{3+}$ for **4**, respectively. It appears that the cholesterol alkene is less susceptible to a radical addition by the thiol than the allyl bonds, likely owing to the increased steric hindrance. In addition, the distinctive peak patterns of the mass spectra reveal the presence of the bromine atom in the final molecules.

Surface plasmon resonance analysis of GMs

Before testing the cholesterol-containing GMs in LNP formulations, their ability to engage in interactions with human lectins was assessed. For this, the targeting ligands were examined in a surface plasmon resonance (SPR) study with five different human lectins. In particular, dendritic cell-specific intercellular adhesion molecule-3-grabbing non-integrin (DC-SIGN), mannose-binding lectin (MBL), mannose-receptor (MR), langerin and liver/lymph node-specific intercellular adhesion molecule-3-grabbing non-integrin (L-SIGN) were used as representative lectins with vital immune system functions.[38–43] Especially DC-SIGN as a receptor associated with macrophages and dendritic cells is a protein of interest for targeted vaccinations.[44] Lectin-binding experiments can provide information about the avidity of the mannosylated targeting ligands towards individual proteins, which provides an indication on how they will perform in cell uptake studies. Consequently, the

Open Access Article. Published on 15 June 2026. Downloaded on 6/15/2026 11:32:43 PM. This article is licensed under a Creative Commons Attribution-NonCommercial 3.0 Unported Licence.

cholesterol-containing GMs were prepared in serial dilutions ranging from 2.2 μM to 70 μM in HBS containing calcium as a binding promoter for c-type lectins. The interaction was measured by flowing the sample solution over the proteins immobilised on the SPR chip, resulting in binding curves of different magnitudes depending on the analyte concentration (Fig. 3A–E). Interaction with lectins could be observed for all samples tested except for MR (SI, Fig. S17), where compounds **2**, **4*S*** and **8*S*** showed unanalysable binding curves with only weak interaction. Generally, binding to MR and L-SIGN generated lower maximum response levels than the other lectins, which can be assigned to the structure of MR with the mannose

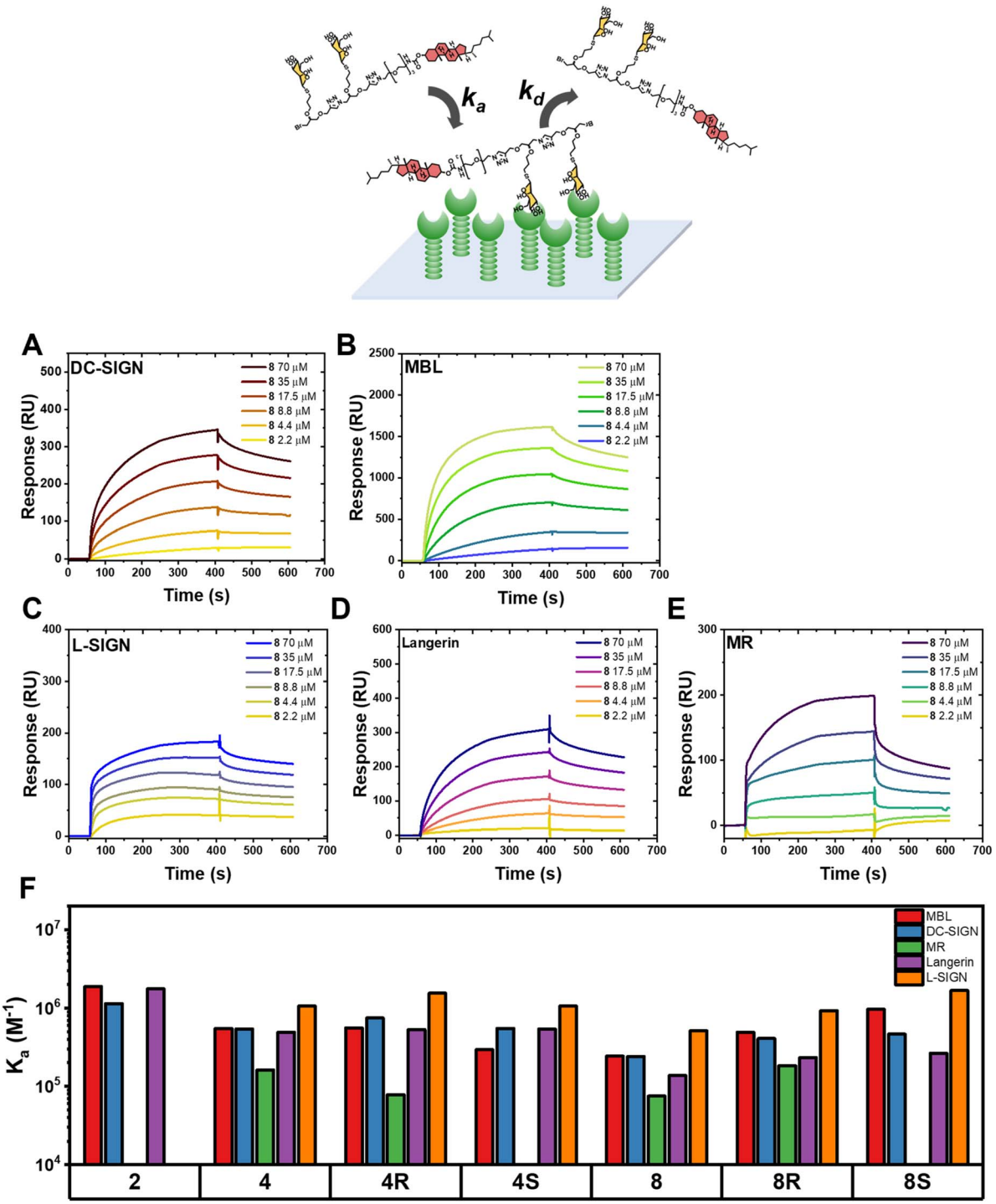

Fig. 3 SPR analysis of the interaction GMs with different lectins. Representative binding curves of compound **8** with (A) DC-SIGN, (B) MBL, (C) L-SIGN, (D) Langerin, (E) mannose receptor (MR). (F) Bar plot of the kinetic association constants (K_a) evaluated from SPR binding curves for cholesterol-containing GMs and lectins using a Langmuir 1 : 1 binding model. Full SPR binding data can be found in the SI.

© 2026 The Author(s). Published by the Royal Society of Chemistry

Open Access Article. Published on 15 June 2026. Downloaded on 6/15/2026 11:32:43 PM. This article is licensed under a Creative Commons Attribution-NonCommercial 3.0 Unported Licence.

binding site located behind the galactose-specific motif.[42,45] In the case of L-SIGN, immobilisation efficiency appeared to be slightly lower than for the other lectins tested, hence, the immobilised proteins are unable to bind the same amount of analyte. The highest response levels were obtained from interaction with MBL, likely induced by an increased number of immobilised binding sites due to oligomer formation of MBL.[46]

Kinetic evaluation of SPR results

The kinetical interpretation of the binding curves obtained from SPR experiments was performed *via* a 1 : 1 Langmuir model to calculate the global kinetic parameters for the interactions to the five lectins (Fig. 3F; SI, Fig. S20, Table S1). The data fitting produces values for the association and dissociation rate constants k_a and k_d, as well as the overall association and dissociation constants, K_a and K_d. Moreover, the calculated R_{max} is reported, representing the theoretical maximal SPR response for a specific analyte–receptor pair for the chosen conditions. Correspondingly, this evaluation provides insight into the avidity of the mannosylated structures to the individual lectins.

Comparison of the association rates (k_a) indicates that association occurs significantly slower for compounds **2**, **4*S*** and **8** with MBL and Langerin than the rest of the tested GMs (SI, Fig. S20A). A similar trend is observed for DC-SIGN with **8** generating the lowest k_a value with this lectin, and for MR, with almost a 3-fold increase in k_a between **8** and **8*R***. L-SIGN, conversely, exhibits the fastest association with **4*S***, although the multivalency is lower than for the octamers. In contrast, dissociation (k_d) of **2** appears to be the slowest for MBL, DC-SIGN and Langerin, despite presenting the lowest number of carbohydrates for multivalent binding (SI, Fig. S20B). Notably slow dissociation was also observed for **4*R*** interacting with L-SIGN, indicating a preference of the protein for a distinct ligand conformation. MR shows generally high values for k_d, owing to weaker binding of the glycoligands with this receptor. Examination of the overall association constants (K_a) underpins the high avidity of **2** to MBL, DC-SIGN and Langerin (Fig. 3F). Additionally, it becomes apparent that MR exhibits the overall weakest adhesion to the GMs. Among the group of octamers, **8*S*** binds the strongest to most lectins, whereas **4*R*** emerges as the most potent ligand within the glycotetramers. Langerin demonstrates preferred binding to glycotetramers over the glycooctamers, which seems unexpected, as higher carbohydrate content is known to lead to synergistic interaction based on the multivalent cluster glycoside effect.[47–49]

Production and physicochemical characterisation of GLNPs

To determine the best concentration of glycooligomers to be included in saRNA LNP formulations, we compared the effect that different concentrations of 5%, 10%, and 15% molar ratios have on the LNP physicochemical properties (Table 1).[50,51] LNPs with increasing molar ratios of glycooligomer exhibited higher hydrodynamic diameters and polydispersity indices (PDI). A RiboGreen assay was performed to quantify the encapsulation efficiency of saRNA into the LNPs.[52] Increasing molar ratios resulted in lower encapsulation efficiencies. Whilst 5 mol% and 10 mol% of glycoligand render satisfactory 94% and 93% encapsulation efficiencies, respectively, the value dropped to 56% at 15 mol% glycosylation. Presumably, the glycoligands interfere with RNA loading, as nucleic acids can interact with sugars *via* carbohydrate–aromatic interactions.[53,54] Additionally, a drop in encapsulation efficiency caused by steric hindrance is a known phenomenon for PEG-lipids, and it seems plausible that the glycooligomers can also induce a similar effect.[55]

In the same set of LNPs, a sample was prepared without adding any PEG lipid to the formulation, as it was reasoned that the glycoligands could potentially replace PEG as a hydrophilic stabiliser, leading to lower risk of anti-PEG immunity.[56] In addition, the PEG chains on the LNP might interfere with the ability of the nanoparticle to interact with the cell surface and shield the mannose units from the respective receptors.[22] Characterisation of the altered formulation (Table 1) reveals that the absence of PEG causes aggregation of particles, leading to a hydrodynamic diameter of >200 nm and PDI > 0.3, thus being inadequate for endocytosis.[57,58] Furthermore, a significant drop in RNA encapsulation has been observed, which is in agreement with mannosylated LNPs in the literature.[21]

Taken together, these results point to the use of saRNA LNPs with 5 mol% of glycooligomers, since this was the only glycosylated formulation to exhibit the desired physicochemical properties, such as hydrodynamic diameter < 100 nm, PDI < 0.3, and an encapsulation efficiency greater than 80%. Having determined the optimal concentration of glycooligomers in LNP formulations, we formulated control and glycosylated C12-200 LNPs using different types of glycooligomers and determined their physicochemical properties (SI, Tables S2 and S3). The control sample without glycoligands exhibited a slightly smaller size (~75 nm) than glycosylated formulations, most of which ranged from 85 to 93 nm. The LNPs that include **2** are the largest in the series with 112 nm. The surface charge gave negative values ranging from −7 to −9.5 mV, indicating successful encapsulation of saRNA, and agreeing with previous literature for PEGylated C12-200 LNPs.[19,56,59] The RiboGreen assay confirmed excellent encapsulation efficiencies of ~95% and above for all samples.

Surface plasmon resonance of LNP formulations with lectins

Confirmation of the successful incorporation of the cholesterol-containing glycoligands into the LNP formulations was performed by SPR. It was presumed that glycosylation would induce lectin binding, whilst the control sample without carbohydrates on the surface would not adhere to the SPR chip. The LNPs used in transfection studies were investigated for their interaction with immobilised MBL and DC-SIGN (Fig. 4). The sensorgrams for C12-200 LNPs with MBL (Fig. 4A) show almost no curvature in the association phase with a dip in response shortly after sample injection followed by a nearly linear association for **8*R*** and **8*S***. No considerable interaction was observed for the LNP control sample, which gave a signal close to the buffer trace. Notably, formulations including **4** and **8** resulted in sensorgrams with lower response levels than the buffer injection and the control sample. Assumably, the amount

Open Access Article. Published on 15 June 2026. Downloaded on 6/15/2026 11:32:43 PM. This article is licensed under a Creative Commons Attribution-NonCommercial 3.0 Unported Licence.

Table 1 Physicochemical properties of saRNA LNPs with glycooligomer at different concentrations (hydrodynamic diameter, PDI, and encapsulation efficiency). LNP: lipid nanoparticle, PEG: polyethylene glycol

Glycooligomer content	Hydrodynamic diameter (nm)	Polydispersity index (PDI)	Encapsulation efficiency (%)
LNP control	64 ± 1	0.19 ± 0.01	97
LNP 5 mol%	70 ± 3	0.26 ± 0.04	94
LNP 10 mol%	100 ± 8	0.39 ± 0.09	93
LNP 15 mol%	83 ± 2	0.31 ± 0.06	56
LNP 15 mol% (PEG-free)	242 ± 96	0.50 ± 0.06	9

of mannose moieties on these LNPs is not sufficient to enable significant interaction with the protein molecules on the chip surface. This could be related to a low yield in the GM incorporation during the microfluidic mixing process. In the dissociation step, the SPR response remains nearly unaltered for all tested samples, indicating that the surface-bound LNP-lectin complex stays intact until the regeneration step. In the case of DC-SIGN (Fig. 4B), the obtained curves are similar in trend to MBL with lower overall response levels, supporting the finding that **8*S*** provides the highest binding levels to lectin receptors. Accordingly, the binding to MBL and DC-SIGN indicates successful carbohydrate coverage of the LNPs.

Luciferase transfection assays with glycosylated saRNA LNP in human cell lines

The functionality of glycosylated LNPs was assessed in transfection experiments by incubating the formulations for 24 h with HEK293T/17 and THP-1 cells (Fig. 5). HEK cells present a well-studied system for transfection experiments, given their high transfectability and lack of RNA sensing mechanisms.[11,60–62] THP-1 is a monocytic cell line that represents an immune cell type and is responsive to saRNA.[63–65] Transfection was allowed to occur for 24 h, upon which luciferin was added to the wells. Since the saRNA encodes for luciferase, the presence of luciferin will induce a luminescence signal, which enables a quantitative readout for the amount of saRNA transfected.[66]

Transfection results for LNPs with varying amounts of added glycooligomer (Fig. 5A) confirmed the enhanced performance of the sample with 5 mol% compared to higher carbohydrate contents. PEG-free LNPs exhibited minimal levels of transfection, which could be explained by suboptimal particle production, as well as differences in delivery pathways due to different physicochemical properties. All GLNP samples presenting different GMs (Fig. 5B) showed good transfection with HEK cells (>10^5 RLU). C12 + **2*R*** and C12 + **8** exhibited 12% and 9% higher transfection levels compared to the LNP control. Likewise, two of the dimers performed better than the set of tetramers. In THP-1 transfection, however, C12 + **4** provided the highest level of expression, whereas C12 + **4*R*** and C12 + **4*S*** presented the lowest values of all samples (Fig. 5C). C12 + **2*S*** showed the best performance within the group of dimers. From the transfection in HEK cells and THP-1, it can be deduced that the stereoconfiguration of the GMs has an influence on the biological performance, albeit not all samples show an improvement over the control. It became apparent that the carbohydrate valency of GMs did not have a major effect on transfection, as some of the octamers exhibit lower levels of luciferase expression than the corresponding dimers and tetramers.

Cytotoxicity assay of glycosylated saRNA LNPs

Upon confirming that the glycosylated saRNA LNP formulations can lead to functional protein expression *in vitro*, we then evaluated their cytotoxicity (Fig. 5D and E). In general, highly efficient systems for nucleic acid delivery tend to exhibit some degree of cytotoxicity.[67] Thus, the glycosylated formulations were tested for potential cytotoxic properties. For this and the

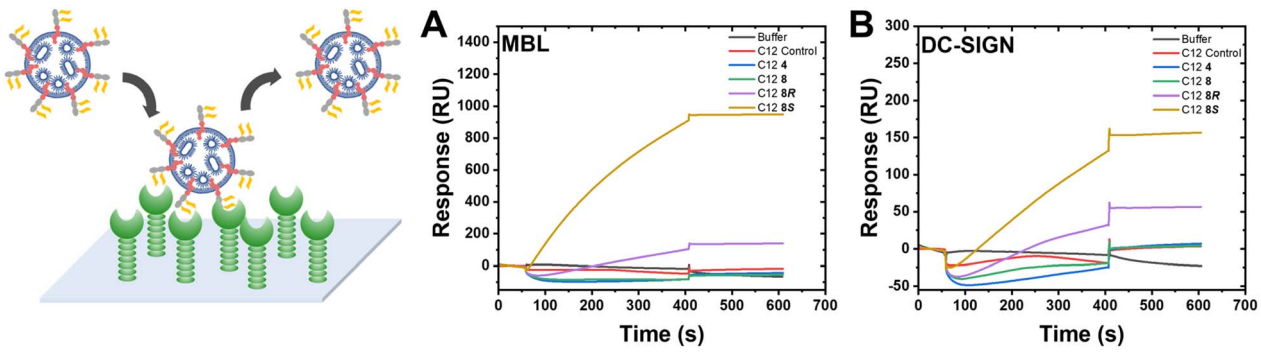

Fig. 4 Lectin binding studies of GLNP formulations. SPR sensorgrams of (A) C12-200 LNP formulations containing different GMs in HBS buffer with MBL, (B) C12-200 LNP formulations containing different GMs in HBS buffer with DC-SIGN.

© 2026 The Author(s). Published by the Royal Society of Chemistry

Open Access Article. Published on 15 June 2026. Downloaded on 6/15/2026 11:32:43 PM.
This article is licensed under a Creative Commons Attribution-NonCommercial 3.0 Unported Licence.

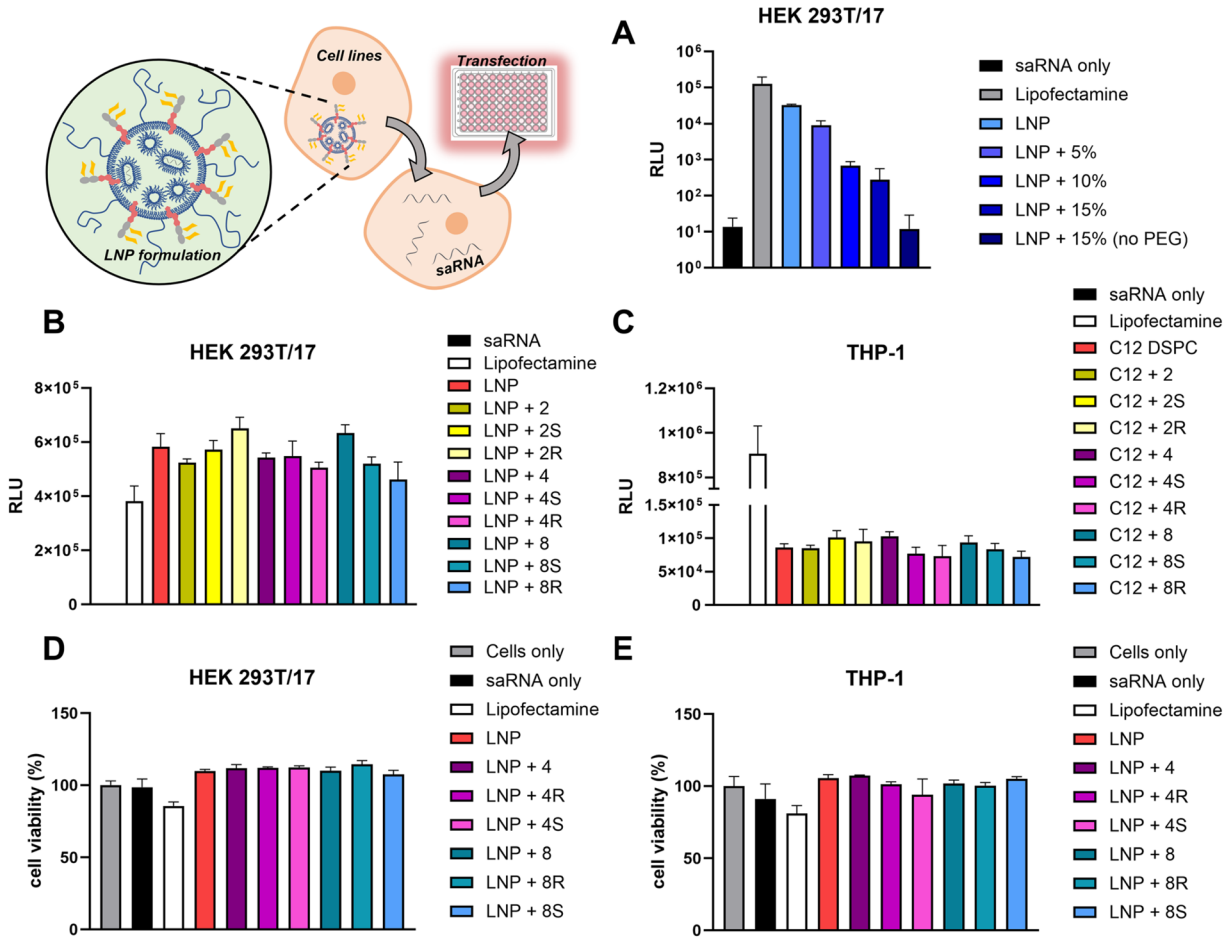

Fig. 5 Luciferase transfection assay results (luminescence intensity) of (A) saRNA LNPs with glycooligomer at various molar ratios. (B) LNP formulations containing different GMs in HEK 293T/17 cell line. (C) LNP formulations containing different GMs in THP-1 cell line. (D/E) Cytotoxicity evaluation of glycosylated saRNA LNP formulations. HEK 293T/17 and THP-1 cells were incubated with the formulations for 24 h. Levels of cellular toxicity were then determined using a CellTiter-Glo® assay. (D) Cell viability of HEK 293T/17 cells, and (E) cell viability of THP-1 cells. Graphs show mean ± s.d. of $n = 3$. LNP: lipid nanoparticle, PEG: polyethylene glycol, RLU: relative light units, saRNA: self-amplifying mRNA.

next experiments, a reduced sample size of glycooligomers was selected, focussing on the compounds with a higher degree of glycosylation. LNPs were incubated with cells in the same conditions as described previously, and their toxicity levels were analysed after 24 h using a CellTiter-Glo® assay. For both HEKs and THP-1s, none of the LNP formulations exhibited cytotoxicity (glycosylated or not), demonstrating the safe applicability of such delivery systems. The positive control lipofectamine, on the other hand, was the only condition to exhibit a more pronounced reduction in cell viability, in both cell types. This is not surprising given that lipofectamine is known for its toxicity.[68]

Cellular transfection efficiency in BMDCs expressing mannose receptors

To further validate the selective delivery of saRNA LNPs to cells that are known for expressing the relevant receptors to the glycooligomers, we analysed transfection in murine bone marrow-derived dendritic cells (BMDCs). Dendritic cells play an important role in the immune system, as they are APCs with the ability to trigger innate immune responses and initiate adaptive immunity.[69,70] BMDCs were chosen as a known model for dendritic cells in transfection assays, as they express mannose receptors.[71–73] Owing to the potent binding of the GMs to DC-SIGN, BMDCs seem a suitable system for the investigation of mannosylated GLNPs. In this assessment, HEK cells were again tested as a positive control for successful transfection, providing additional information about the reproducibility of the delivery system (Fig. 6A). In HEK cells, C12 + **8** displayed higher levels of luciferase expression, in absolute numbers, than both control samples. In contrast, C12 + **8*S*** exhibited a lower amount of luminescence, indicating reduced preference for this glycoligand.

Examination of the transfection results with BMDCs revealed the highest signal among the tested formulations was achieved by C12 + **8** (Fig. 6B). GLNPs formulations exhibited transfection levels in the same range of the control LNP. Although BMDCs are more difficult to transfect than HEKs, this result was unexpected, as the GLNPs do not seem to induce the desired boost in transfection. The performance of GLNPs for C12-200

Open Access Article. Published on 15 June 2026. Downloaded on 6/15/2026 11:32:43 PM.
This article is licensed under a Creative Commons Attribution-NonCommercial 3.0 Unported Licence.

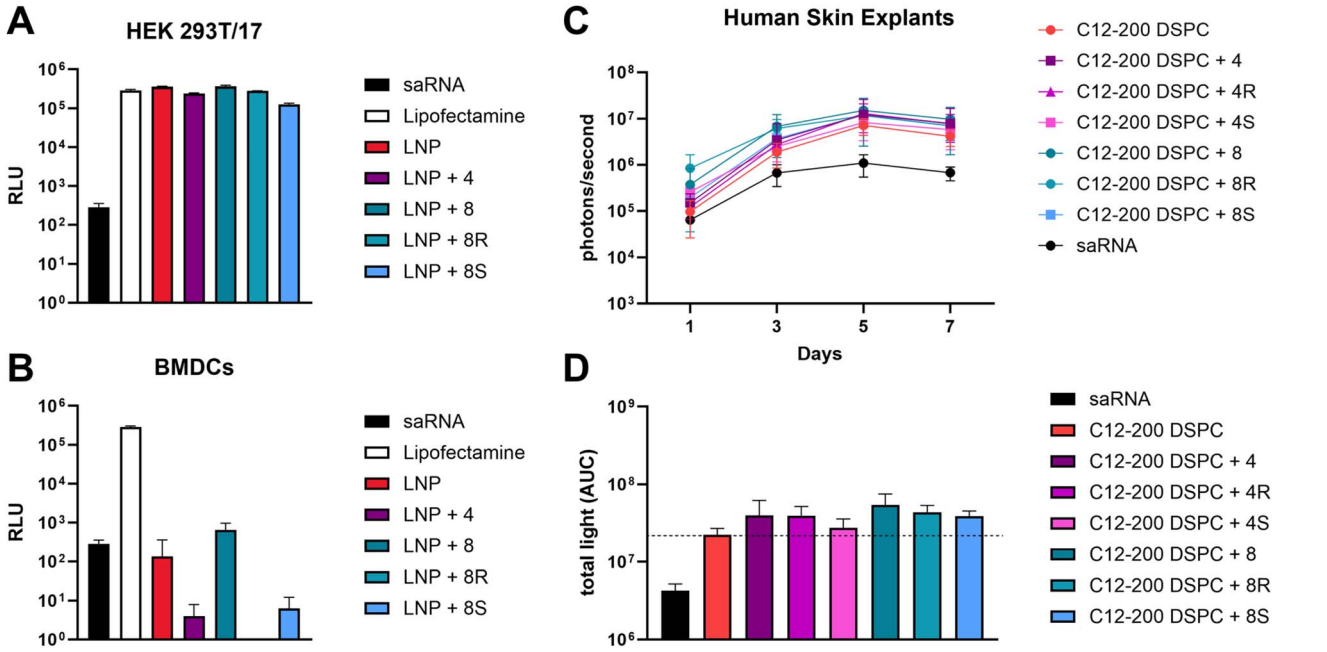

Fig. 6 Transfection assay results (luminescence intensity) of (A) C12-200 DSPC formulations containing different GMs in HEK 293T/17 cell line. (B) C12-200 DSPC formulations containing different GMs in BMDCs. All results were recorded after 24 h of transfection. Graph shows mean ± s.d. of $n = 3$. (C) SaRNA expression levels in human skin explants transfected with glycosylated LNPs over seven days, which was used to calculate (D) the area under the curve (AUC) for each formulation. Graph shows mean ± s.d. of $n = 3$.

varies according to the type of glycooligomer, thus it can be deduced that glycoligand stereoconfiguration modulates interaction with BMDCs in C12-200 formulations, however this needs to be further explored.

Glycosylated saRNA LNPs result in high levels of expression in human skin explants *ex vivo*

Since transfection of glycosylated saRNA LNPs with murine BMDCs did not result in increased expression levels, we sought to determine transfection efficiency in an *ex vivo* model of greater relevance to human vaccination (Fig. 6C and D). Human skin explants were employed as an *ex vivo* model due to their previously demonstrated translational potential for saRNA vaccines.[19,74]

In this study, explants were transfected with 1 μg of luciferase saRNA encapsulated inside LNPs with different glycosylated ligands, and transfection efficiency was assessed by bioluminescence imaging. LNPs with ligand **8** exhibited approximately 2-fold higher levels of saRNA expression in skin explants, compared to the non-glycosylated LNP. Furthermore, in absolute numbers, glycosylated formulations induced higher expression levels than the non-glycosylated LNP. However, the use of human skin explants as a model for assessing transfection efficiency seems promising for the evaluation of functionalised RNA LNP formulations. Differences between human skin explants and murine BMDCs could be explained by interspecies differences, as well as by intrinsic differences between *in vitro* and *ex vivo* models, considering that each model will have specific cell types and proportions of each.[75,76]

Conclusions

In this work, the synthesis of cholesterol-containing glycomacromolecules with varying stereoconfiguration and number of carbohydrates based on IEG has been described. CD spectroscopy was used to confirm the chiral integrity of the glycooligomers after synthesis completion. The GMs have been investigated by SPR for their ability to bind to human lectins MBL, DC-SIGN, L-SIGN, MR and Langerin. It was found that in this specific case glycovalency was not the main driving force for lectin binding, as altering the number of mannose units from two to four or eight did not drastically affect the magnitude of avidity. However, different association and dissociation kinetics were observed for the variations in stereochemistry of the oligomer backbone, indicating preferential binding of specific glycooligomer–lectin pairs. This is in agreement with previous literature and further biological cell transfection studies were employed to test the selective targeting abilities of the system. Therein, cholesterol end groups of the glycooligomers act as an anchoring point for the fabrication of glycosylated LNPs with different surface carbohydrate valency and stereoconfiguration. Successful incorporation of the oligomers into the LNPs was confirmed by SPR. Additionally, saRNA-based transfection assays with HEK293T/17, THP-1 and BMDCs revealed good functional protein expression enabled by the formulations. For HEK cells in particular, differences in expression levels indicate that cellular uptake can potentially be modulated by altering the chirality of the glycoligands. The glycovalency, on the other hand, seemed to have only a minor influence on the transfection. Additionally, glycosylated LNPs exhibited higher

© 2026 The Author(s). Published by the Royal Society of Chemistry

Open Access Article. Published on 15 June 2026. Downloaded on 6/15/2026 11:32:43 PM. This article is licensed under a Creative Commons Attribution-NonCommercial 3.0 Unported Licence.

expression levels in human skin explants compared to control experiments, highlighting the benefit of glycosylation in these formulations. Ultimately, these findings pave the way for more selective therapeutics relying on carbohydrate-mediated nucleic acid delivery.

Experimental section

Materials

Azobisisobutyronitrile (AIBN) (Sigma-Aldrich, 98%), sodium azide (Sigma-Aldrich, >99%), tetrabutyl ammonium fluoride (1.0 M in THF, Sigma-Aldrich), anhydrous tetrahydrofuran (THF) (99.9%, Acros Organics, extra dry), anhydrous acetonitrile (99.9%, Acros Organics, extra dry), *N*,*N*,*N*′,*N*″,*N*″-pentamethyl diethylenetriamine (PMDETA) (Sigma-Aldrich, 99%), copper(I) bromide (CuBr) (Sigma-Aldrich, 98%), 4-(2-hydroxyethyl)-1-piperazineethanesulfonic acid (HEPES, Sigma-Aldrich), sodium methoxide (25w% in MeOH, Sigma-Aldrich), 3-(13-azido-5,8,11-trioxa-2-azatridecanoate)cholesterol (cholesteryl-TEG-azide, Sigma-Aldrich) were all used as received. Lectins (DC-SIGN, L-SIGN (DC-SIGNR), MBL, Langerin and Mannose Receptor 1) were purchased from Bio-Techne (USA) and used as received. Dialysis tubing was purchased from SpectraPor (USA) and rinsed with DI-water before use. 2,3,4,6-tetra-*O*-acetyl-1-thio-β-D-mannopyranose (Ac_4ManSH) was synthesised according to the literature.[77]

Methods

Nuclear magnetic resonance. All NMR spectra were measured at 298 K on a Bruker HD300 or HD400 in $CDCl_3$, D_2O or DMSO-d6.

High-performance liquid chromatography (HPLC). HPLC was performed on an Agilent 1260 Infinity II system (DAD detection at 210 nm) equipped with an Agilent InfinityLab Poroshell 120 EC-C18 (4.6 mmID, 100 mmL, 2.7 μm) column with an isocratic elution mixture H_2O/MeCN 1% (+0.04% TFA).

High resolution electron-spray ionisation mass spectrometry (ESI-MS). HR ESI-MS spectra were measured on a Bruker Compact Q-TOF in positive ion mode.

Circular dichroism spectroscopy (CD). CD spectra were acquired on a Jasco J-1500 spectrometer at 25 °C using a 1 mm cuvette. Sample solutions were prepared at a concentration of 1.0 mg mL^{-1} and filtered through a 0.2 μm nylon filter. If the CD scan showed a high-tension voltage (HT) of over 700 V, the sample was diluted down to stay below that threshold. A total of 128 scans were recorded.

Surface plasmon resonance (SPR). SPR was used to determine the extent of interaction between the GMs and lectins. Samples were analysed on a BIAcore T200 system (Cytiva Life Sciences). The lectins (25 μg mL^{-1}) were immobilised *via* a standard amino coupling protocol onto a CM5 sensor chip that was activated by flowing a 1 : 1 mixture of 0.1 M *N*-hydroxysuccinimide (NHS) and 0.4 M *N*-ethyl-*N*′ (dimethylaminopropyl)-carbodiimide (EDC) over the chip for 5 min at 20 °C at a flow rate of 5 μL min^{-1} after system equilibration with HEPES-buffered saline (HBS) buffer (10 mM HEPES pH 7.4, 150 mM NaCl, 5 mM $CaCl_2$). Subsequently, channels 1 (blank), 2, 3 and 4 were blocked by flowing a solution of ethanolamine (1 M pH 8.5) for 10 min at 5 μL min^{-1} to block remaining reactive groups on the channels. Sample solutions were prepared at varying concentrations (70 μM to 2.2 μM) in the same HBS buffer to calculate the binding kinetics. Sensorgrams for each sample concentration were recorded at 20 °C with a flow rate of 25 μL min^{-1}. Injection of GM solution 350 s (on period) was followed by 200 s of buffer alone (off period). Regeneration of the sensor chip surfaces was performed using a solution of 10 mM HEPES pH 7.4, 150 mM NaCl, 10 mM EDTA, 0.01% Tween20. All binding curves were subjected to double referencing by subtracting the signal of a reference channel without protein on the chip and the signal of a blank buffer injection. Kinetic data was evaluated using a 1 : 1 langmuir binding model in the BIA evaluation 3.1 software. SPR samples for LNP formulations were prepared by diluting 40 μL of the formulation stock solution in BSA with 160 μL of HBS.

***In vitro* transcription (IVT) of self-amplifying mRNA.** Venezuelan Equine Encephalitis Virus (VEEV)-derived self-amplifying mRNA (saRNA) used in this study encoded for firefly luciferase (fLuc). The first step consisted of linearising the plasmid DNA template using MluI (New England BioLabs, UK) for 3 h at 37 °C. DNA linearisation was confirmed by agarose gel electrophoresis. Next, RNA synthesis was done *via in vitro* transcription (IVT) reactions using the HiScribe kit (Invitrogen, Thermo Fisher Scientific, UK), according to the manufacturer's instructions. Transcripts were purified by lithium chloride (LiCl) precipitation. Initially, transcripts were added to a LiCl solution overnight at −20 °C and centrifuged the following day at 14 000 rpm for 20 min at 4 °C. Pellets were resuspended in 70% ethanol and centrifuged at 14 000 rpm for 5 min at 4 °C. The ethanol was removed, pellets were allowed to dry for 5 min, and transcripts were reconstituted in ultrapure H_2O. RNA quantification was done using a NanoDrop One (Thermo Fisher Scientific, UK) and RNA integrity was evaluated by RNA gel electrophoresis.

LNP formulation. The following lipids were used for preparation of LNPs with and without polymers: C12-200 (Corden Pharma, Switzerland), 1,2-distearoyl-*sn*-glycero-3-phosphocholine (DSPC) (Avanti® Polar Lipids, US), cholesterol (plant-derived) (Avanti® Polar Lipids, US) and 1,2-dimyristoyl-*sn*-glycero-3-phosphoethanolamine-*N*-[methoxy(polyethylene glycol)-2000] (ammonium salt) (DMPE-PEG2000) (Avanti® Polar Lipids, US).

C12-200 LNPs were prepared with C12-200, DSPC, cholesterol, and DMPE-PEG2000 at a molar ratio of 35 : 16 : 46.5 : 2.5, at an RNA to lipid ratio of 1 : 55 (w/w). Glycopolymer stock solutions were prepared in RNase-free water and added at different molar ratios from 2% to 15%. The content of glycopolymer in the glycosylated LNPs replaced cholesterol in the corresponding amounts.

saRNA solutions were prepared in 50 mM sodium acetate (Sigma®, US) and 100 mM sodium chloride buffer (Sigma®, US) at pH = 5.5. LNPs were formulated on a NanoAssemblr (Precision NanoSystems Incorporated, Vancouver, BC, Canada) using a flow rate ratio of RNA:lipid of 3 : 1 and a total flow rate of 8

Open Access Article. Published on 15 June 2026. Downloaded on 6/15/2026 11:32:43 PM. This article is licensed under a Creative Commons Attribution-NonCommercial 3.0 Unported Licence.

mL min^{-1}. The formulated material was then diluted in Dulbecco's phosphate-buffered saline (DPBS) 1× (Gibco, UK) in approximately 5 times the volume of the total formulation. This diluted sample was spun down using VivaSpin 6 filter tubes with a molecular weight cut-off (MWCO) of 10 kDa (Sartorius, Germany) at 4000 rpm and 18 °C until the desired concentration was achieved. Samples were stored at 4 °C until usage.

RNA encapsulation efficiency by RiboGreen assay. The quantification of saRNA encapsulated inside lipid nanoparticles was analysed using a Quant-iT RiboGreen assay (ThermoFisher, UK) according to Precision NanoSystems' protocol. Briefly, samples were diluted to a concentration in the range of 6 μg mL^{-1} and added 1 : 1 in either 1× TE Buffer or Triton X-100, using a black 96-well Costar® plate (ThermoFisher, UK). Samples were incubated at 37 °C for 10 min to allow for the lysis of LNPs and then kept for 5 min at room temperature. RiboGreen reagent was prepared at a 1 : 100 dilution in 1× TE buffer, and 100 μL was added per well. An RNA standard curve was also prepared as recommended by the protocol. Fluorescence intensity was analysed on a microplate reader (BMG LABTECH, UK) at an excitation of 480 nm and emission of 520 nm. The concentration of total saRNA and saRNA on the outside (non-encapsulated) was calculated based on the standard curve. The concentration of encapsulated saRNA was calculated by subtraction (total saRNA minus non-encapsulated saRNA). The percentage of encapsulation efficiency (EE) was calculated as:

$$EE\ (\%) = 100 \times (\text{RNA encapsulated/RNA added to assay})$$

LNP physicochemical characterization. *Z*-Average diameter and zeta potential were analysed using a Zetasizer Nano ZS (Malvern Instruments, UK). Samples were equilibrated at room temperature and then diluted 1 : 100 in DPBS 1× (Gibco, UK), in a total of 850 μL. DTS1070 cuvettes were used, and the parameters were as follows: material refractive index of 1.529, absorbance of 0.010, dispersant viscosity of 0.8820 cP, refractive index of 1.330 and dielectric constant of 79.

Cell line and culture conditions. HEK293T/17 cells (ATCC, US) were routinely grown in Dulbecco's Modified Eagle's Medium (DMEM) (Gibco, Thermo Fisher, UK) supplemented with 10% (v/v) foetal bovine serum (FBS), 1% (v/v) L-glutamine, and 1% (v/v) penicillin/streptomycin (Thermo Fisher, UK), at 37 °C under 5% CO_2. When confluent, cells were washed with DPBS 1× (Gibco, UK) and treated with trypsin (TrypLE Express 1×) (Gibco, UK) for seeding in new culture flasks (Corning, US).

THP-1 cells (ATCC, US) were routinely grown in RPMI-1640 Medium (Sigma, UK) supplemented with 10% (v/v) foetal bovine serum (FBS), 1% (v/v) L-glutamine, and 1% (v/v) penicillin/streptomycin (Thermo Fisher, UK), at 37 °C under 5% CO_2. When confluent, the whole cell suspension in culture media was centrifuged at 1750 rpm for 5 min, and the pellet was re-suspended in fresh RPMI-1640 medium for seeding in new culture flasks (Corning, US).

Establishment of BMDCs culture. For the culture of bone marrow cells, the bone marrow was initially harvested from BALB/c mice by removing the excess fat and muscle tissue from the legs. Samples were kept on ice in Petri dishes (Thermo Fisher Scientific, UK) containing RPMI medium (Sigma, UK) and later sterilised by placing them in 70% ethanol for 1–2 min on ice. Next, bones were transferred to a Petri dish containing fresh complete RPMI medium and flushed using microfine insulin needles (BD Biosciences, US), for collection of bone marrow cells. The medium was then transferred to 50 mL conical tubes (Falcon®, Corning, US) and spun down at 400 g for 5 min. The pellet was resuspended in 1 mL of ACK Lysing buffer (Lonza, US) and incubated for 2 min at RT. Then, 9 mL of complete RPMI medium was added, and the solution was filtered using 70 μm strain filters (Falcon®, Corning, US). The solution was spun down again, and the pellet obtained was resuspended in complete RPMI medium. Cells were plated at 1 × 10^6 cells per mL in Petri dishes with complete RPMI medium and supplemented with recombinant murine GM-CSF (PeproTech®, UK) 40 μg mL^{-1} at 1 : 1000 dilution, and 2-Mercaptoethanol 50 mM (Gibco, UK) at 1 : 1000 dilution too. The cell culture medium was changed every 3 days by removing half of the medium and replacing it with an equal volume of fresh medium and adding fresh growth factors. Upon 7 days, cells were checked under the microscope for differentiation and plated in 96-well plates (Falcon®, Corning, US) at a concentration of 50 × 10^3 cells per well in 100 μL.

Cell transfection assay. On the day before the experiment, cells were seeded in 96-well plates at the following concentrations: HEK 293T/17 at 50 × 10^3 cells per well, THP-1 cells at 80 × 10^3 cells per well, and BMDCs at 50 × 10^3 cells per well. For the evaluation of transfection efficiency, a dose of 100 ng of saRNA-LNPs was added to each well containing the appropriate fully supplemented media, and transfection was allowed to occur for 24 hours. Next, 50 μL of the medium was removed from each well and replaced with 50 μL of Bright-Glo™ luciferin substrate (Promega, UK). After 5 min, the whole 100 μL was transferred to white plates (Falcon®, US), and luminescence intensity was analysed using a FLUOstar Omega plate reader (BMG LABTECH, UK).

Cellular viability assessment with CellTiter-Glo® 2.0 assay. HEK 293T/17 cells were seeded at 50 × 10^3 cells per well and THP-1 cells at 80 × 10^3 cells per well. Cells were transfected the next day with 100 ng of saRNA encapsulated inside lipid nanoparticles. Cells were incubated with saRNA LNPs for 24 h. Plates were equilibrated at room temperature for 30 min and an equal volume of the CellTiter-Glo® 2.0 (Promega, UK) reagent was added to the wells (100 μL). Contents were mixed for 2 min using an orbital shaker (Jencons Scientific Ltd, UK), and plates were incubated for 10 min at room temperature. The total volume was transferred to a white plate (Falcon®, US), and luminescence intensity was analysed on a FLUOstar Omega plate reader (BMG LABTECH, UK).

Human skin explants culture and bioluminescence imaging. Human skin tissue samples were obtained from healthy donors at Charing Cross Hospital, Imperial NHS Trust, London, UK. Patients signed an informed consent form, and procedures followed the Local Research Ethics Committee protocols. Skin tissue was originally from elective mastectomy and abdominoplasty surgeries. Initially, the subcutaneous fat layer was

© 2026 The Author(s). Published by the Royal Society of Chemistry

Open Access Article. Published on 15 June 2026. Downloaded on 6/15/2026 11:32:43 PM. This article is licensed under a Creative Commons Attribution-NonCommercial 3.0 Unported Licence.

removed, and the explants of 1 cm × 1 cm were made by using a scalpel (Swann-Morton™, Fisher Scientific, UK). Explants were placed in 12-well plates with 2 mL of DMEM (Gibco, Thermo Fisher UK) supplemented with 10% (v/v) foetal bovine serum (FBS), 1% (v/v) L-glutamine, and 1% (v/v) penicillin/streptomycin (Thermo Fisher, UK). Cell culture media was replaced daily. To analyse saRNA expression in human skin tissue, explants were transfected with 1 μg of fLuc encapsulated within control and glycosylated LNP formulations. Samples were injected intradermally with 1 μg of saRNA-LNP in 50 μL using Micro-fine insulin needles (BD Biosciences, UK), at a 15° angle in a controlled manner. For acquisition of bioluminescence imaging, media was replaced with 950 μL of DMEM (Gibco, Thermo Fisher, UK) and 50 μL of IVISbrite D-luciferin Bioluminescent Substrate in RediJect Solution (Revvity, UK) and explants were incubated for 10 minutes. Image acquisition was performed using the Ami HT Optical Imaging System (Spectral Instruments Imaging, US) using a suitable exposure, and image analysis was done using the Aura Image Analysis Software version 4.0.8 (Spectral Instruments Imaging, US).

Synthetic procedures

Typical procedure for CuAAC of triazole backbone with chol-TEG-azide. Under inert atmosphere, allyl-IEG-dimer **1** (0.021 g, 0.05 mmol, 1 eq.) was dissolved in dry THF (0.25 mL) and the solution was degassed with an N_2 stream for 2 min. Tetrabutylammonium fluoride solution (1 M in THF, 0.053 mL, 1.1 eq.) was added and the mixture was stirred for 2 h at room temperature. In a separate vial, cholesteryl-TEG-azide (0.038 g, 0.06 mmol, 1.2 eq.) was dissolved in dry THF (0.25 mL), degassed, and added to the reaction mixture. Copper(I) bromide (0.001 g, 0.008 mmol 0.15 eq.) and PMDETA (1.6 μL, 0.008 mmol, 0.15 eq.) were added and the mixture was heated to 45 °C for 18 h. After completion, the solvent was removed under reduced pressure and the residue dissolved in DCM (10 mL). The organic layer was washed with H_2O (3 × 10 mL), dried over $MgSO_4$, filtered and the solvent removed under reduced pressure. The product **2A** (0.044 g) was obtained as a viscous oil and used in the next step without further purification.

^{1}H NMR (400 MHz, $CDCl_3$): δ(ppm) 7.76 (s, 1H, Ar–*H*), 7.65 (s, 1H, Ar–*H*), 6.03–5.83 (m, 1H, C*H*=CH_2), 5.80–5.62 (m, 1H, C*H*=CH_2), 5.34 (bs, 2H, Chol-C=C*H*), 5.26–5.07 (m, 4H, CH=CH_2), 4.71–4.61 (m, 4H, OCH_2-Ar), 4.60–4.52 (m, 4H), 4.51–4.35 (m, 4H), 4.30–4.20 (m, 3H), 4.10 (s, 2H), 4.05–3.96 (m, 3H), 3.93–3.81 (m, 4H), 3.66 (s, 4H), 3.65–3.57 (m, 13H), 3.57–3.47 (m, 7H), 3.41–3.26 (m, 5H), 2.40–2.19 (m, 4H), 2.08–1.90 (m, 5H), 1.90–1.75 (m, 7H), 1.61–1.39 (m, 16H), 1.38–1.28 (m, 8H), 1.24 (s, 6H), 1.17–1.08 (m, 11H), 1.02–0.95 (m, 16H), 0.90 (d, J = 6.4 Hz, 8H), 0.85 (d, J = 6.5 Hz, 14H), 0.66 (6H).

Typical procedure for thiol–ene reaction with thiomannose. Under inert atmosphere, **2A** (0.016 g, 0.015 mmol, 1 eq.) was dissolved in dry acetonitrile (0.4 mL) and Ac_4ManSH (0.066 g, 0.180 mmol, 12 eq.) and AIBN (0.001 g, 0.008 mmol, 0.5 eq.) were added. The suspension was degassed with a stream of nitrogen for 5 min and was heated to 70 °C for 18 h. Afterwards the solvent was removed under reduced pressure, and the residue was dissolved in methanol (0.5 mL). Sodium methoxide solution (25w% in MeOH, 20 μL) was added and the mixture was stirred at r.t. for 2 h. A mixture of H_2O/DMSO 1 : 1 (5 mL) was added, and the solution was transferred into a dialysis bag (MWCO: 100–500 Da) and dialysed against H_2O for 48 h. Lyophilisation afforded the product **2** (0.010 g, 46%) as a white solid.

^{1}H NMR (400 MHz, DMSO-*d*6): δ(ppm) 8.09 (s, 1H, Ar–*H*), 8.05 (s, 1H, Ar–*H*), 7.06 (t, J = 5.7 Hz, 1H, N*H*), 5.32 (bs, 1H, Chol-C=C*H*), 4.80–4.70 (m, 4H, Man-C*H*), 4.69–4.63 (m, 2H, Man-C*H*), 4.60 (s, 1H), 4.56 (s, 3H, OCH_2-Ar), 4.54–4.47 (m, 6H, OCH_2), 4.46–4.41 (m, 2H), 4.41–4.33 (m, 2H), 4.33–4.24 (m, 2H), 3.85–3.78 (m, 3H), 3.70–3.60 (m, 5H), 3.54–3.44 (m, 14H, TEG-CH_2), 3.29 (bs, 4H), 3.13–3.00 (m, 5H), 2.69–2.61 (m, 2H), 2.54 (s, 5H), 2.35–2.13 (m, 4H), 1.99–1.86 (m, 3H), 1.86–1.70 (m, 5H), 1.68–1.58 (m, 3H), 1.57–1.42 (m, 8H), 1.42–1.28 (m, 7H), 1.23 (s, 5H), 1.15–0.98 (m, 10H), 0.95 (s, 5H), 0.89 (d, J = 6.4 Hz, 4H), 0.84 (d, J = 6.6 Hz, 8H), 0.64 (s, 3H).

Author contributions

J. B. and B. D.-B. performed the research experiments. R. J. S. and C. R. B. supervised the research and acquired funding. All authors analysed the experimental data, edited, and commented on the manuscript.

Conflicts of interest

There are no conflicts to declare.

Data availability

Synthesis procedures, NMR spectra, ESI-MS, LNP characterisation results, SPR sensorgrams and kinetic data can be found in the supplementary information (SI). Supplementary information is available. See DOI: https://doi.org/10.1039/d6sc03833f.

Acknowledgements

J. B. and B. D.-B. thank the BIOMOLMACS ITN, a European project funded by the European Union's Horizon 2020 research and innovation programme under the Marie Skłodowska-Curie grant agreement no. 859416 for funding. The authors acknowledge use of the SPR instrument provided by the Bio-Analytical Shared Resource Laboratories within the School of Life Sciences/Warwick Medical School, University of Warwick. R. J. S. is supported in part by the NIHR Imperial Biomedical Research Centre (BRC).

References

1 S. M. Hoy, Patisiran: First Global Approval, *Drugs*, 2018, **78**(15), 1625–1631, DOI: 10.1007/s40265-018-0983-6.
2 R. Verbeke, I. Lentacker, S. C. De Smedt and H. Dewitte, The dawn of mRNA vaccines: the COVID-19 case, *J. Controlled*

Open Access Article. Published on 15 June 2026. Downloaded on 6/15/2026 11:32:43 PM. This article is licensed under a Creative Commons Attribution-NonCommercial 3.0 Unported Licence.

Release, 2021, **333**, 511–520, DOI: 10.1016/j.jconrel.2021.03.043.

3 J. A. Kulkarni, P. R. Cullis and R. van der Meel, Lipid Nanoparticles Enabling Gene Therapies: From Concepts to Clinical Utility, *Nucleic Acid Ther.*, 2018, **28**(3), 146–157, DOI: 10.1089/nat.2018.0721.

4 Y. Suzuki, K. Hyodo, Y. Tanaka and H. Ishihara, siRNA-lipid nanoparticles with long-term storage stability facilitate potent gene-silencing *in vivo*, *J. Controlled Release*, 2015, **220**(Pt A), 44–50, DOI: 10.1016/j.jconrel.2015.10.024.

5 K. Godbout and J. P. Tremblay, Delivery of RNAs to Specific Organs by Lipid Nanoparticles for Gene Therapy, *Pharmaceutics*, 2022, **14**(10), 2129, DOI: 10.3390/pharmaceutics14102129.

6 Y. Zhao and L. Huang, Lipid nanoparticles for gene delivery, *Adv. Genet.*, 2014, **88**, 13–36, DOI: 10.1016/B978-0-12-800148-6.00002-X.

7 S. C. Semple, R. Leone, C. J. Barbosa, Y. K. Tam and P. J. C. Lin, Lipid Nanoparticle Delivery Systems to Enable mRNA-Based Therapeutics, *Pharmaceutics*, 2022, **14**(2), 398, DOI: 10.3390/pharmaceutics14020398.

8 G. Tavernier, O. Andries, J. Demeester, N. N. Sanders, S. C. De Smedt and J. Rejman, mRNA as gene therapeutic: how to control protein expression, *J. Controlled Release*, 2011, **150**(3), 238–247, DOI: 10.1016/j.jconrel.2010.10.020.

9 M. N. Fleeton, M. Chen, P. Berglund, G. Rhodes, S. E. Parker, M. Murphy, G. J. Atkins and P. Liljestrom, Self-replicative RNA vaccines elicit protection against influenza A virus, respiratory syncytial virus, and a tickborne encephalitis virus, *J. Infect. Dis.*, 2001, **183**(9), 1395–1398, DOI: 10.1086/319857.

10 A. K. Blakney, P. F. McKay, B. I. Yus, Y. Aldon and R. J. Shattock, Inside out: optimization of lipid nanoparticle formulations for exterior complexation and *in vivo* delivery of saRNA, *Gene Ther.*, 2019, **26**(9), 363–372, DOI: 10.1038/s41434-019-0095-2.

11 G. Hayes, B. Dias-Barbieri, G. Yilmaz, R. J. Shattock and C. R. Becer, Poly(2-oxazoline)/saRNA Polyplexes for Targeted and Nonviral Gene Delivery, *Biomacromolecules*, 2023, **24**(11), 5142–5151, DOI: 10.1021/acs.biomac.3c00683.

12 A. J. Geall, A. Verma, G. R. Otten, C. A. Shaw, A. Hekele, K. Banerjee, Y. Cu, C. W. Beard, L. A. Brito, T. Krucker, *et al.*, Nonviral delivery of self-amplifying RNA vaccines, *Proc. Natl. Acad. Sci. U. S. A.*, 2012, **109**(36), 14604–14609, DOI: 10.1073/pnas.1209367109.

13 X. Hou, T. Zaks, R. Langer and Y. Dong, Lipid nanoparticles for mRNA delivery, *Nat. Rev. Mater.*, 2021, **6**(12), 1078–1094, DOI: 10.1038/s41578-021-00358-0.

14 S. Kimura and H. Harashima, On the mechanism of tissue-selective gene delivery by lipid nanoparticles, *J. Controlled Release*, 2023, **362**, 797–811, DOI: 10.1016/j.jconrel.2023.03.052.

15 J. Kim, Y. Eygeris, R. C. Ryals, A. Jozic and G. Sahay, Strategies for non-viral vectors targeting organs beyond the liver, *Nat. Nanotechnol.*, 2024, **19**(4), 428–447, DOI: 10.1038/s41565-023-01563-4.

16 X. Cheng and R. J. Lee, The role of helper lipids in lipid nanoparticles (LNPs) designed for oligonucleotide delivery, *Adv. Drug Delivery Rev.*, 2016, **99**(Pt A), 129–137, DOI: 10.1016/j.addr.2016.01.022.

17 C. Hald Albertsen, J. A. Kulkarni, D. Witzigmann, M. Lind, K. Petersson and J. B. Simonsen, The role of lipid components in lipid nanoparticles for vaccines and gene therapy, *Adv. Drug Delivery Rev.*, 2022, **188**, 114416, DOI: 10.1016/j.addr.2022.114416.

18 M. Jeong, Y. Lee, J. Park, H. Jung and H. Lee, Lipid nanoparticles (LNPs) for *in vivo* RNA delivery and their breakthrough technology for future applications, *Adv. Drug Delivery Rev.*, 2023, **200**, 114990, DOI: 10.1016/j.addr.2023.114990.

19 A. K. Blakney, P. Deletic, P. F. McKay, C. R. Bouton, M. Ashford, R. J. Shattock and A. Sabirsh, Effect of complexing lipids on cellular uptake and expression of messenger RNA in human skin explants, *J. Controlled Release*, 2021, **330**, 1250–1261, DOI: 10.1016/j.jconrel.2020.11.033.

20 Q. Cheng, T. Wei, L. Farbiak, L. T. Johnson, S. A. Dilliard and D. J. Siegwart, Selective organ targeting (SORT) nanoparticles for tissue-specific mRNA delivery and CRISPR-Cas gene editing, *Nat. Nanotechnol.*, 2020, **15**(4), 313–320, DOI: 10.1038/s41565-020-0669-6.

21 R. Goswami, D. Chatzikleanthous, G. Lou, F. Giusti, A. Bonci, M. Taccone, M. Brazzoli, S. Gallorini, I. Ferlenghi, F. Berti, *et al.*, Mannosylation of LNP Results in Improved Potency for Self-Amplifying RNA (SAM) Vaccines, *ACS Infect. Dis.*, 2019, **5**(9), 1546–1558, DOI: 10.1021/acsinfecdis.9b00084.

22 R. Goswami, D. T. O'Hagan, R. Adamo and B. C. Baudner, Conjugation of Mannans to Enhance the Potency of Liposome Nanoparticles for the Delivery of RNA Vaccines, *Pharmaceutics*, 2021, **13**(2), 240, DOI: 10.3390/pharmaceutics13020240.

23 J. O'Sullivan, J. Munoz-Munoz, G. Turnbull, N. Sim, S. Penny and S. Moschos, Beyond GalNAc! Drug delivery systems comprising complex oligosaccharides for targeted use of nucleic acid therapeutics, *RSC Adv.*, 2022, **12**(32), 20432–20446, DOI: 10.1039/d2ra01999j.

24 M. Kim, M. Jeong, S. Hur, Y. Cho, J. Park, H. Jung, Y. Seo, H. A. Woo, K. T. Nam, K. Lee, *et al.*, Engineered ionizable lipid nanoparticles for targeted delivery of RNA therapeutics into different types of cells in the liver, *Sci. Adv.*, 2021, **7**(9), eabf4398, DOI: 10.1126/sciadv.abf4398.

25 J. Lei, S. Qi, X. Yu, X. Gao, K. Yang, X. Zhang, M. Cheng, B. Bai, Y. Feng, M. Lu, *et al.*, Development of Mannosylated Lipid Nanoparticles for mRNA Cancer Vaccine with High Antigen Presentation Efficiency and Immunomodulatory Capability, *Angew. Chem., Int. Ed.*, 2024, **63**(13), e202318515, DOI: 10.1002/anie.202318515.

26 M. Hartweg, Y. Jiang, G. Yilmaz, C. M. Jarvis, H. V. Nguyen, G. A. Primo, A. Monaco, V. P. Beyer, K. K. Chen, S. Mohapatra, *et al.*, Synthetic Glycomacromolecules of Defined Valency, Absolute Configuration, and Topology

 © 2026 The Author(s). Published by the Royal Society of Chemistry

Open Access Article. Published on 15 June 2026. Downloaded on 6/15/2026 11:32:43 PM. This article is licensed under a Creative Commons Attribution-NonCommercial 3.0 Unported Licence.

Distinguish between Human Lectins, *JACS Au*, 2021, **1**(10), 1621–1630, DOI: 10.1021/jacsau.1c00255.
27 S. J. Richards and M. I. Gibson, Toward Glycomaterials with Selectivity as Well as Affinity, *JACS Au*, 2021, **1**(12), 2089–2099, DOI: 10.1021/jacsau.1c00352.
28 M. H. Stenzel, Glycopolymers for Drug Delivery: Opportunities and Challenges, *Macromolecules*, 2022, **55**(12), 4867–4890, DOI: 10.1021/acs.macromol.2c00557.
29 T. Zhao, R. Terracciano, J. Becker, A. Monaco, G. Yilmaz and C. R. Becer, Hierarchy of Complex Glycomacromolecules: From Controlled Topologies to Biomedical Applications, *Biomacromolecules*, 2022, **23**(3), 543–575, DOI: 10.1021/acs.biomac.1c01294.
30 J. C. Barnes, D. J. Ehrlich, A. X. Gao, F. A. Leibfarth, Y. Jiang, E. Zhou, T. F. Jamison and J. A. Johnson, Iterative exponential growth of stereo- and sequence-controlled polymers, *Nat. Chem.*, 2015, **7**(10), 810–815, DOI: 10.1038/nchem.2346.
31 M. R. Golder, Y. Jiang, P. E. Teichen, H. V. Nguyen, W. Wang, N. Milos, S. A. Freedman, A. P. Willard and J. A. Johnson, Stereochemical Sequence Dictates Unimolecular Diblock Copolymer Assembly, *J. Am. Chem. Soc.*, 2018, **140**(5), 1596–1599, DOI: 10.1021/jacs.7b12696.
32 Y. Jiang, M. R. Golder, H. V. Nguyen, Y. Wang, M. Zhong, J. C. Barnes, D. J. Ehrlich and J. A. Johnson, Iterative Exponential Growth Synthesis and Assembly of Uniform Diblock Copolymers, *J. Am. Chem. Soc.*, 2016, **138**(30), 9369–9372, DOI: 10.1021/jacs.6b04964.
33 M. Z. C. Hatit, C. P. Seath, A. J. B. Watson and G. A. Burley, Strategy for Conditional Orthogonal Sequential CuAAC Reactions Using a Protected Aromatic Ynamine, *J. Org. Chem.*, 2017, **82**(10), 5461–5468, DOI: 10.1021/acs.joc.7b00545.
34 Y.-L. Li, D.-P. Song, L. Pan, Z. Ma and Y.-S. Li, Facile functionalization of isotactic polypropylene *via* click chemistry, *Polym. Chem.*, 2019, **10**(46), 6368–6378, DOI: 10.1039/c9py01225g.
35 J. Becker, R. Terracciano, G. Yilmaz, R. Napier and C. R. Becer, Step-Growth Glycopolymers with a Defined Tacticity for Selective Carbohydrate-Lectin Recognition, *Biomacromolecules*, 2023, **24**(4), 1924–1933, DOI: 10.1021/acs.biomac.3c00133.
36 R. Lloyd. J. J. K. Snyder and J. W. Dolan, *Introduction to Modern Liquid Chromatography*, John Wiley & Sons, Inc., 3 edn, 2009, pp. 297–298.
37 G. Palla, C18 Reversed-phase liquid chromatographic determination of invert sugar, sucrose, and raffinose, *Anal. Chem.*, 2002, **53**(12), 1966–1967, DOI: 10.1021/ac00235a065.
38 R. M. Steinman, DC-SIGN: a guide to some mysteries of dendritic cells, *Cell*, 2000, **100**(5), 491–494, DOI: 10.1016/s0092-8674(00)80684-4.
39 E. A. Koppel, K. P. van Gisbergen, T. B. Geijtenbeek and Y. van Kooyk, Distinct functions of DC-SIGN and its homologues L-SIGN (DC-SIGNR) and mSIGNR1 in pathogen recognition and immune regulation, *Cell. Microbiol.*, 2005, **7**(2), 157–165, DOI: 10.1111/j.1462-5822.2004.00480.x.
40 U. S. Khoo, K. Y. Chan, V. S. Chan and C. L. Lin, DC-SIGN and L-SIGN: the SIGNs for infection, *J. Mol. Med.*, 2008, **86**(8), 861–874, DOI: 10.1007/s00109-008-0350-2.
41 M. W. Turner, The role of mannose-binding lectin in health and disease, *Mol. Immunol.*, 2003, **40**(7), 423–429, DOI: 10.1016/s0161-5890(03)00155-x.
42 L. Martinez-Pomares, The mannose receptor, *J. Leukoc. Biol.*, 2012, **92**(6), 1177–1186, DOI: 10.1189/jlb.0512231.
43 M. van der Vlist and T. B. Geijtenbeek, Langerin functions as an antiviral receptor on Langerhans cells, *Immunol. Cell Biol.*, 2010, **88**(4), 410–415, DOI: 10.1038/icb.2010.32.
44 Y. van Kooyk, W. W. Unger, C. M. Fehres, H. Kalay and J. J. Garcia-Vallejo, Glycan-based DC-SIGN targeting vaccines to enhance antigen cross-presentation, *Mol. Immunol.*, 2013, **55**(2), 143–145, DOI: 10.1016/j.molimm.2012.10.031.
45 F. Mastrotto, M. Pirazzini, S. Negro, A. Salama, L. Martinez-Pomares and G. Mantovani, Sulfation at Glycopolymer Side Chains Switches Activity at the Macrophage Mannose Receptor (CD206) *In Vitro* and *In Vivo*, *J. Am. Chem. Soc.*, 2022, **144**(50), 23134–23147, DOI: 10.1021/jacs.2c10757.
46 J. S. Presanis, M. Kojima and R. B. Sim, Biochemistry and genetics of mannan-binding lectin (MBL), *Biochem. Soc. Trans.*, 2003, **31**(4), 748–752, DOI: 10.1042/bst0310748.
47 J. J. Lundquist and E. J. Toone, The cluster glycoside effect, *Chem. Rev.*, 2002, **102**(2), 555–578, DOI: 10.1021/cr000418f.
48 C. R. Becer, The glycopolymer code: synthesis of glycopolymers and multivalent carbohydrate-lectin interactions, *Macromol. Rapid Commun.*, 2012, **33**(9), 742–752, DOI: 10.1002/marc.201200055.
49 M. Mammen, S.-K. Choi and G. M. Whitesides, Polyvalent Interactions in Biological Systems: Implications for Design and Use of Multivalent Ligands and Inhibitors, *Angew. Chem., Int. Ed.*, 1998, **37**(20), 2754–2794, DOI: 10.1002/(sici)1521-3773(19981102)37:20<2754::Aid-anie2754>3.0.Co;2-3.
50 D. Kim, Y. Wu, G. Shim and Y. K. Oh, Lipid Nanoparticle-Mediated Lymphatic Delivery of Immunostimulatory Nucleic Acids, *Pharmaceutics*, 2021, **13**(4), 490, DOI: 10.3390/pharmaceutics13040490.
51 J. Y. Zeng, S. Lingesh, N. B. Krishnan, B. S. Y. Loong, M. Liu, Q. Chen and Y. Y. Yang, Cholesterol-Derived Mannosylated Polypeptide-Formed Lipid Nanoparticles for Efficient *in Vivo* mRNA Delivery, *Small Methods*, 2025, **9**(6), e2401712, DOI: 10.1002/smtd.202401712.
52 L. J. Jones, S. T. Yue, C. Y. Cheung and V. L. Singer, RNA quantitation by fluorescence-based solution assay: RiboGreen reagent characterization, *Anal. Biochem.*, 1998, **265**(2), 368–374, DOI: 10.1006/abio.1998.2914.
53 M. D. Disney and P. H. Seeberger, Aminoglycoside microarrays to explore interactions of antibiotics with RNAs and proteins, *Chem.–Eur. J.*, 2004, **10**(13), 3308–3314, DOI: 10.1002/chem.200306017.
54 J. L. Asensio, A. Arda, F. J. Canada and J. Jimenez-Barbero, Carbohydrate-aromatic interactions, *Acc. Chem. Res.*, 2013, **46**(4), 946–954, DOI: 10.1021/ar300024d.
55 L. Zhang, B. Y. L. Seow, K. H. Bae, Y. Zhang, K. C. Liao, Y. Wan and Y. Y. Yang, Role of PEGylated lipid in lipid

Open Access Article. Published on 15 June 2026. Downloaded on 6/15/2026 11:32:43 PM. This article is licensed under a Creative Commons Attribution-NonCommercial 3.0 Unported Licence.

nanoparticle formulation for *in vitro* and *in vivo* delivery of mRNA vaccines, *J. Controlled Release*, 2025, **380**, 108–124, DOI: 10.1016/j.jconrel.2025.01.071.

56 K. Knop, R. Hoogenboom, D. Fischer and U. S. Schubert, Poly(ethylene glycol) in drug delivery: pros and cons as well as potential alternatives, *Angew. Chem., Int. Ed.*, 2010, **49**(36), 6288–6308, DOI: 10.1002/anie.200902672.

57 I. Canton and G. Battaglia, Endocytosis at the nanoscale, *Chem. Soc. Rev.*, 2012, **41**(7), 2718–2739, DOI: 10.1039/c2cs15309b.

58 M. Sousa de Almeida, E. Susnik, B. Drasler, P. Taladriz-Blanco, A. Petri-Fink and B. Rothen-Rutishauser, Understanding nanoparticle endocytosis to improve targeting strategies in nanomedicine, *Chem. Soc. Rev.*, 2021, **50**(9), 5397–5434, DOI: 10.1039/d0cs01127d.

59 K. Poornima, A. Puri, A. Gupta and X. Lu, Understanding the Stealth Properties of PEGylated lipids: A Mini-Review, *Int. J. Lipids*, 2020, **1**(2), 1–20, DOI: 10.14302/issn.2835-513X.ijl-20-3457.

60 P. Thomas and T. G. Smart, HEK293 cell line: a vehicle for the expression of recombinant proteins, *J. Pharmacol. Toxicol. Methods*, 2005, **51**(3), 187–200, DOI: 10.1016/j.vascn.2004.08.014.

61 C. B. Ferreira, R. P. Sumner, M. T. Rodriguez-Plata, J. Rasaiyaah, R. S. Milne, A. J. Thrasher, W. Qasim and G. J. Towers, Lentiviral Vector Production Titer Is Not Limited in HEK293T by Induced Intracellular Innate Immunity, *Mol. Ther. Methods Clin. Dev.*, 2020, **17**, 209–219, DOI: 10.1016/j.omtm.2019.11.021.

62 E. Warga, J. Anderson, M. Tucker, E. Harris and J. Elmer, Transcriptomic analysis of the innate immune response to *in vitro* transfection of plasmid DNA, *Mol. Ther. Nucleic Acids*, 2023, **31**, 43–56, DOI: 10.1016/j.omtn.2022.11.025.

63 H. Bosshart and M. Heinzelmann, THP-1 cells as a model for human monocytes, *Ann. Transl. Med.*, 2016, **4**(21), 438, DOI: 10.21037/atm.2016.08.53.

64 W. Chanput, J. J. Mes and H. J. Wichers, THP-1 cell line: an *in vitro* cell model for immune modulation approach, *Int. Immunopharmacol.*, 2014, **23**(1), 37–45, DOI: 10.1016/j.intimp.2014.08.002.

65 G. Molina-Olvera, C. I. Rivas-Ortiz, A. Schcolnik-Cabrera, A. I. Castillo-Rodal and Y. Lopez-Vidal, RNA Microarray-Based Comparison of Innate Immune Phenotypes between Human THP-1 Macrophages Stimulated with Two BCG Strains, *Int. J. Mol. Sci.*, 2022, **23**(9), 4525, DOI: 10.3390/ijms23094525.

66 R. L. Ball, K. A. Hajj, J. Vizelman, P. Bajaj and K. A. Whitehead, Lipid Nanoparticle Formulations for Enhanced Co-delivery of siRNA and mRNA, *Nano Lett.*, 2018, **18**(6), 3814–3822, DOI: 10.1021/acs.nanolett.8b01101.

67 K. Paunovska, D. Loughrey and J. E. Dahlman, Drug delivery systems for RNA therapeutics, *Nat. Rev. Genet.*, 2022, **23**(5), 265–280, DOI: 10.1038/s41576-021-00439-4.

68 T. Wang, L. M. Larcher, L. Ma and R. N. Veedu, Systematic Screening of Commonly Used Commercial Transfection Reagents towards Efficient Transfection of Single-Stranded Oligonucleotides, *Molecules*, 2018, **23**(10), 2564, DOI: 10.3390/molecules23102564.

69 M. L. Kapsenberg, Dendritic-cell control of pathogen-driven T-cell polarization, *Nat. Rev. Immunol.*, 2003, **3**(12), 984–993, DOI: 10.1038/nri1246.

70 C. J. Howard, B. Charleston, S. A. Stephens, P. Sopp and J. C. Hope, The role of dendritic cells in shaping the immune response, *Anim. Health Res. Rev.*, 2004, **5**(2), 191–195, DOI: 10.1079/ahr200468.

71 E. J. McKenzie, P. R. Taylor, R. J. Stillion, A. D. Lucas, J. Harris, S. Gordon and L. Martinez-Pomares, Mannose receptor expression and function define a new population of murine dendritic cells, *J. Immunol.*, 2007, **178**(8), 4975–4983, DOI: 10.4049/jimmunol.178.8.4975.

72 S. T. T. Schetters, L. J. W. Kruijssen, M. H. W. Crommentuijn, H. Kalay, J. Ochando, J. M. M. den Haan, J. J. Garcia-Vallejo and Y. van Kooyk, Mouse DC-SIGN/CD209a as Target for Antigen Delivery and Adaptive Immunity, *Front. Immunol.*, 2018, **9**, 990, DOI: 10.3389/fimmu.2018.00990.

73 S. Burgdorf, V. Lukacs-Kornek and C. Kurts, The mannose receptor mediates uptake of soluble but not of cell-associated antigen for cross-presentation, *J. Immunol.*, 2006, **176**(11), 6770–6776, DOI: 10.4049/jimmunol.176.11.6770.

74 A. K. Blakney, P. F. McKay, B. Ibarzo Yus, J. E. Hunter, E. A. Dex and R. J. Shattock, The Skin You Are In: Design-of-Experiments Optimization of Lipid Nanoparticle Self-Amplifying RNA Formulations in Human Skin Explants, *ACS Nano*, 2019, **13**(5), 5920–5930, DOI: 10.1021/acsnano.9b01774.

75 S. Tahtinen, A. J. Tong, P. Himmels, J. Oh, A. Paler-Martinez, L. Kim, S. Wichner, Y. Oei, M. J. McCarron, E. C. Freund, *et al.*, IL-1 and IL-1ra are key regulators of the inflammatory response to RNA vaccines, *Nat. Immunol.*, 2022, **23**(4), 532–542, DOI: 10.1038/s41590-022-01160-y.

76 J. Mestas and C. C. Hughes, Of mice and not men: differences between mouse and human immunology, *J. Immunol.*, 2004, **172**(5), 2731–2738, DOI: 10.4049/jimmunol.172.5.2731.

77 Y. Ishido, N. Kanbayashi, N. Fujii, T. A. Okamura, T. Haino and K. Onitsuka, Folding control of a non-natural glycopeptide using saccharide-coded structural information for polypeptides, *Chem. Commun.*, 2020, **56**(18), 2767–2770, DOI: 10.1039/c9cc10030j.

© 2026 The Author(s). Published by the Royal Society of Chemistry